JMEPEG (2009) 18:475–478
DOI: 10.1007/s11665-009-9396-8

1059-9495/$19.00

Influence of Quenching Rates on Equiatomic NiTi Ribbons Fabricated by Melt-Spinning

K. Mehrabi, M. Bruncko, B.J. McKay, and A.C. Kneissl

(Submitted September 18, 2008; in revised form December 16, 2008)

Quenching rates, in terms of circumferential wheel speed in melt-spinning, play an important role in the resultant characteristics of the ribbons. In this study, the influence of various wheel speeds on ribbon dimensions, cross-sectional microstructures, and crystallographic phases within samples were investigated. The Ni-50.3at.%Ti melt-spun ribbons were produced under 200 mbar He atmosphere at wheel speeds of 5-30 ms^{-1} using a quartz crucible coated internally with Y_2O_3. The different wheel speeds led to different sample dimensions and cooling rates. The microstructures of the samples were observed using optical microscopy and TEM, while the shape memory effect of samples and the existing phases were studied by differential scanning calorimetry, x-ray diffraction, and tensile tests.

Keywords melt-spinning, NiTi, shape memory alloys, wheel speed

1. Introduction

NiTi shape memory alloys (SMAs) have received considerable research attention and are widely used because they combine special functional properties with high mechanical strength (Ref 1). These characteristics are due to the martensitic transformation and its reversion, which can be activated by thermal or mechanical loads. SMAs show good corrosion resistance, wear resistance, and high specific electric resistance (which is beneficial for direct current heating) and can be exploited many times before functional or structural fatigue limit service life (Ref 2).

A very promising field for high-volume applications of SMAs in the near future lies in actuator technology, since with a shape memory element, a pre-determined response can be obtained very easily by thermal or electric stimulus. Especially the possibility to realize even complicated movements with an element of simple design and compact size makes shape memory actuators very attractive. There is also a trend to very small-dimensioned shape memory elements which could be used as microactuators. The application of rapid solidification can drastically change the microstructure, improving the ductility and shape memory characteristics, leading to small-dimensioned samples (Ref 3).

Generally there are several advantages of rapid solidification (quenching rate varies from 10^3 up to 10^7 K/s (Ref 4)) over the slower conventional solidification techniques. These are an ability to form metastable phases, increasing the solubility above the equilibrium solubility, decreasing the segregation of additions, and refining the microstructure. It is considered that all of these effects have been attempted to improve shape memory effects in the rapidly solidified ribbons.

Many physical properties of melt-spun ribbons, as well as their microstructures, sensitively depend on the values of the processing parameters such as the wheel speed, gas pressure, melt temperature, nozzle-wheel gap, etc. (Ref 5). As known from the literature (e.g. Ref 6), cooling rates are proportional to the wheel speed. In the present study, the microstructure and shape memory behavior of NiTi alloy ribbons, fabricated at different cooling rates by melt-spinning, were investigated.

2. Experimental Procedure

In this study, an investigation of the microstructures and shape memory effect of Ni-50.3at.%Ti melt-spun ribbons was carried out. First of all, the alloy was prepared in ingot form by vacuum arc-melting technique on a water-cooled copper crucible in a reduced Ar atmosphere. To ensure homogeneous SMAs, arc-melting was repeated three times for each alloy.

The melt-spun ribbons were produced under a 200 mbar He atmosphere using quartz-glass crucibles with a nozzle diameter of 0.9 mm and coated internally with Y_2O_3. By applying an Ar overpressure of 90 mbar within the crucible, the melt was ejected onto the surface of a polished Cu wheel (200 mm diameter) having a circumferential wheel speed of 5-30 m/s. The distance between the nozzle and the wheel surface was 2 mm.

Specimens for metallographic investigation were cut from the longitudinal cross sections of melt-spun ribbons. They were

This article is an invited paper selected from presentations at Shape Memory and Superelastic Technologies 2008, held September 21-25, 2008, in Stresa, Italy, and has been expanded from the original presentation.

K. Mehrabi, M. Bruncko, and **A.C. Kneissl**, Department of Physical Metallurgy and Materials Testing, University of Leoben, Leoben, Austria; **M. Bruncko**, Faculty of Mechanical Engineering, University of Maribor, Maribor, Slovenia; and **B.J. McKay**, Department of Metallurgy, University of Leoben, Leoben, Austria. Contact e-mail: kambiz.mehrabi@unileoben.ac.at.

ground on SiC paper to a final mesh size of 2400 and polished. The samples were etched with conventional and wipe-etching in a solution containing HF:HNO_3:H_2O = 1:4:5 and studied by optical microscopy using interference contrast. For TEM experiments, thin discs (3 mm in diameter) were mechanically ground and dimpled to a thickness of 25-30 μm. Ion-milling was then performed on the samples until electron transparency was achieved. The energy of the Ar+ ions was 3.6 keV, the angle to the surface of the specimen was ±4°, and the specimen was kept at a rotation rate of 3 rpm during ion-milling. Conventional TEM studies were carried out with an acceleration voltage of 120 kV.

The phase transformation temperatures were measured using a Mettler DSC 821e device (Mettler Toledo GmbH, Schwerzenbach, CH). Thermograms were recorded under static air from −40 to 180 °C at a heating/cooling rate of 10 °C/min. A circular sample disc was cut with a punch (5 mg), put in a 20 μL aluminum pan, and closed with a perforated lid. The crystallographic structure was determined using Bragg-Brentano x-ray diffraction with CuKα radiation at room temperature. Tensile specimens with gauge size of 55 mm in length, 2 mm in width, and 80 μm in thickness were cut from the melt-spun ribbons and tested on a universal testing machine with a crosshead speed of 0.1 mm/min at room temperature.

3. Results and Discussion

Figure 1(a) shows an optical micrograph of a conventionally etched ribbon (wheel speed 15 m/s). The microstructure is primarily single phase, with small amounts of secondary phase distributed in the matrix. Since the stoichiometric range of NiTi is very narrow at low temperatures, it is quite usual that the material contains precipitates of a second phase. By EDX analysis these particles were found to be Ti_2Ni precipitates. In this picture because of the very fine and sophisticated microstructure, it is not easy to characterize the martensitic microstructure with conventional etching method. Figure 1(b) shows the martensitic structure of the same ribbon after wipe-etching using interference contrast. From Fig. 1(a) it seems that the grain size is about 5-10 μm but it is hard to relate this to the martensitic structure seen in Fig. 1(b), therefore we cannot be sure that this is the real grain size. The same observations have also been found by Undisz et al. (Ref 7).

Furthermore, TEM was employed to investigate the martensitic structures of the NiTi ribbons, which were too fine to be sufficiently resolved with optical microscopy, especially in the ribbons fabricated at the higher wheel speed. Figure 2 displays a fine martensitic structure (B19′ phase) of a melt-spun ribbon (wheel speed 30 m/s) with nano-sized twin boundaries.

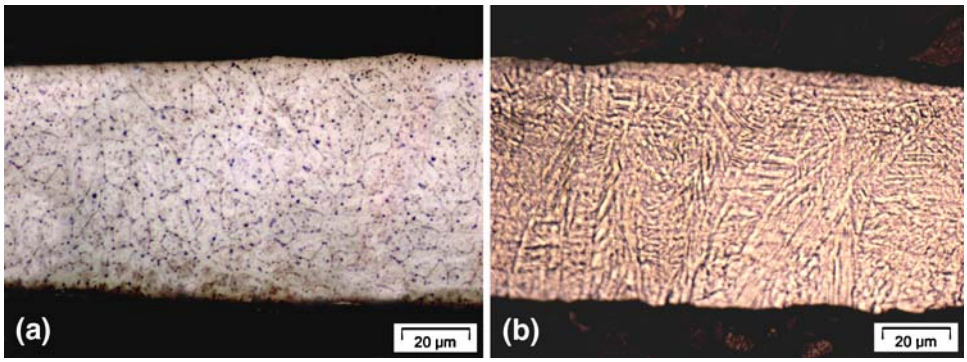

Fig. 1 Optical microstructures of melt-spun ribbon: (a) conventionally etched surface and (b) martensite structure after wipe-etching using interference contrast

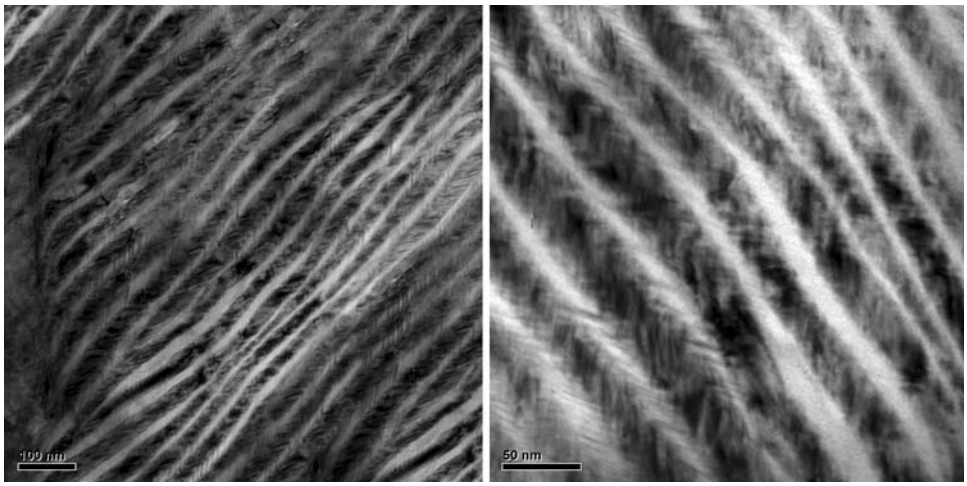

Fig. 2 TEM images of the B19′ martensite of a melt-spun shape memory alloy

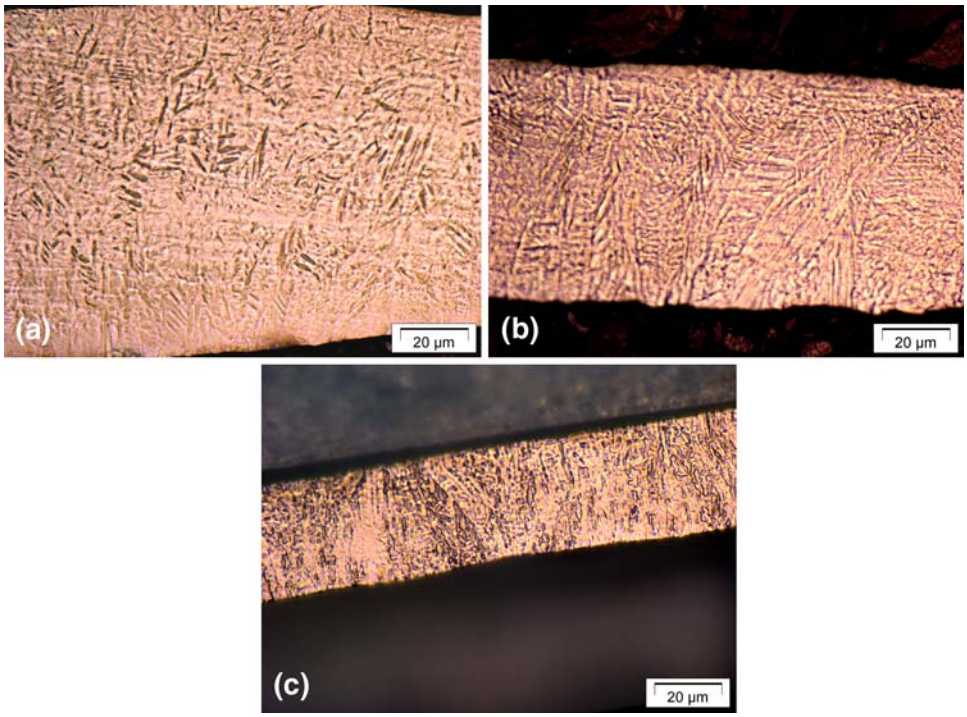

Fig. 3 Optical cross-sectional view of NiTi ribbons at various wheel speeds, wipe-etching using interference contrast: (a) 5 m/s, (b) 15 m/s, and (c) 30 m/s

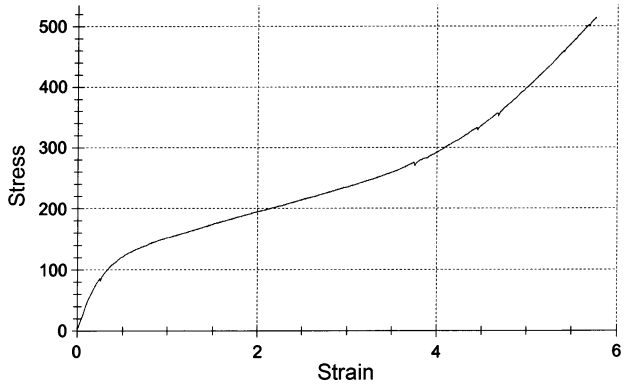

Fig. 4 Stress-strain curve of the melt-spun ribbon; martensite plateau

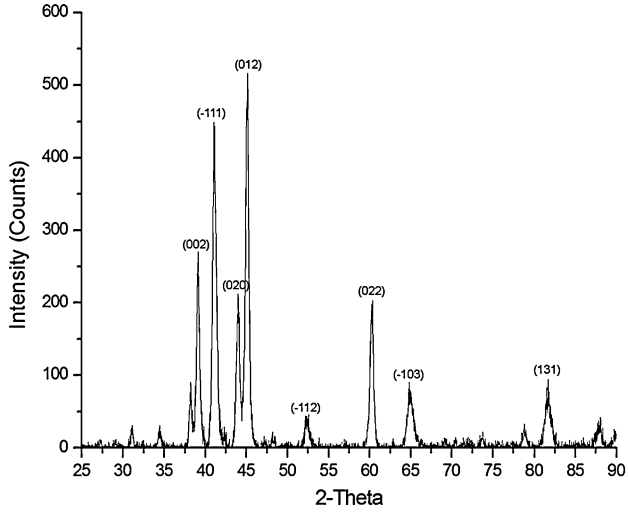

Fig. 5 XRD patterns of the ribbons, B19′ phase

The variation of cooling rates was achieved by the speed of the Cu wheel that was changed from 5 to 30 m/s while the melt-spinning temperature was fixed at 1350 °C. Figure 3 shows the cross-sectional view of ribbons at various wheel speeds. An increase of the wheel speed from 5 to 30 m/s results in a decrease of the ribbon thickness from 100 to 20 µm. As the increase of the wheel speed leads to a reduced ribbon thickness, the cooling rate increases.

Tensile tests of melt-spun ribbons fabricated at various wheel speeds show clearly the martensitic plateau even without subsequent heat treatment (e.g. Fig. 4). The shape memory one-way effect is about 4% in these samples.

The results of XRD experiments were obtained from the free side of the ribbons. The results also show that all of the ribbons manufactured at the different wheel speeds are crystalline and martensitic (e.g. Fig. 5). No transition from crystalline phase to amorphous phase with increasing cooling rate even at the wheel speed of 30 m/s could be found.

Figure 6 displays the DSC curves for the melt-spun ribbons at speeds of 5, 15, and 30 m/s. Figure 6(a) shows the phase transformation for the lowest wheel speed and therefore the lowest cooling rate while Fig. 6(b) and (c) represents the higher wheel speeds and cooling rates. There is not much difference in the transformation temperatures but a slight shift to higher martensite transformation temperatures which is not in accordance with other observations, e.g. Ref 8, 9. These papers deal

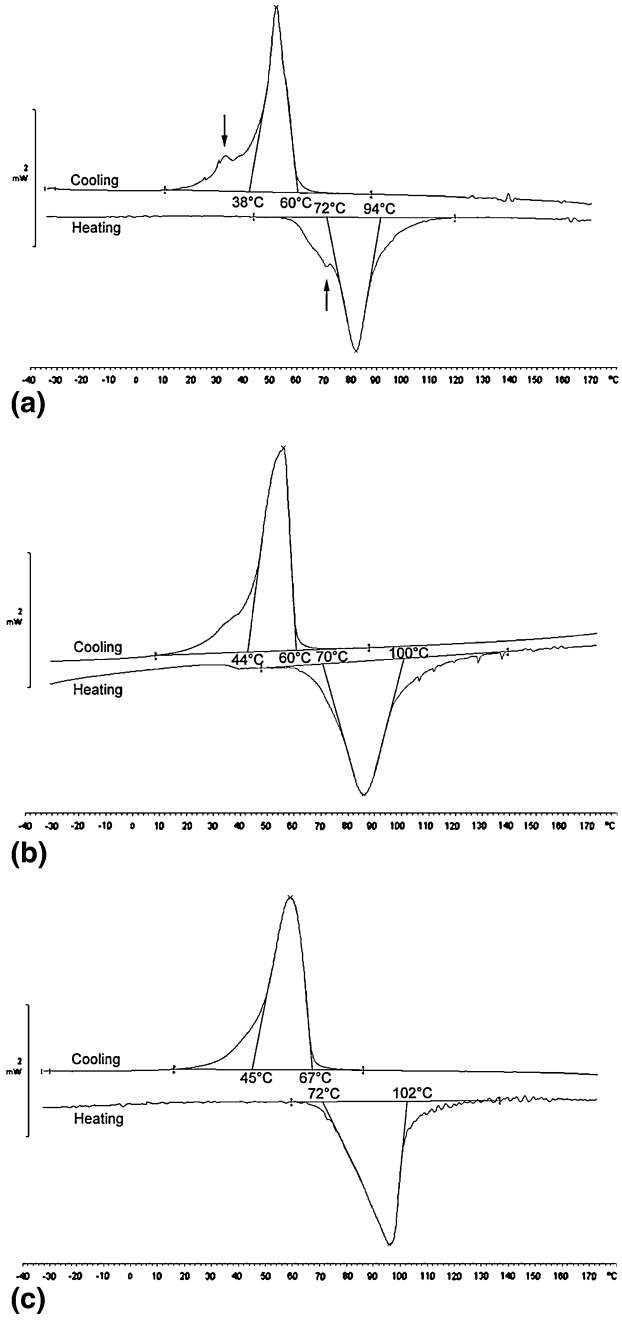

Fig. 6 DSC curves of NiTi ribbons at various wheel speeds: (a) 5 m/s, (b) 15 m/s, and (c) 30 m/s

with Cu-based SMAs and obtain lower martensite transformation temperatures with decreasing grain size. In this study, it was not possible to make quantitative comparisons of the grain size. However, the martensitic microstructure became finer with increasing wheel speed. The very slight increase of the martensite transformation temperatures could be caused probably by higher internal stresses because of higher cooling rates. It also seems that there are additional peaks at the lower cooling rates, especially in the final stage of the martensitic transformation (evident in Fig. 6a). Perhaps these additional peaks could be attributed to the fact that transformation temperatures of the chilled side are different from those of the free side of the ribbons.

4. Conclusions

The work of this paper has shown that the melt-spin technique is able to produce samples with good shape memory properties immediately after cooling even without subsequent heat treatment. The higher the wheel speed, the smaller the thickness of the resulting ribbon and therefore the higher the cooling rate. With increasing cooling rate the microstructure gets finer and finer and therefore metallographic preparation was not easy at all. Using wipe-etching and interference contrast, it was possible to reveal the fine martensitic structure; by TEM investigations also the twin boundaries of the martensitic structure could be shown. XRD and DSC investigations revealed that all samples were fully martensitic at room temperature. At the higher cooling rates, the martensite transformation temperatures were very slightly raised, probably due to higher internal stresses. The material with very fine microstructure has also good mechanical properties (strength and ductility) and therefore exhibits good potential for future microactuator applications.

References

1. J. Frenzel, Z. Zhang, K. Neuking, and G. Eggeler, High Quality Vacuum Induction Melting of Small Quantities of NiTi Shape Memory Alloys in Graphite Crucibles, *J. Alloys Compd.*, 2004, **385**, p 214–223
2. S. Miyazaki, T.W. Duerig, K.N. Melton, D. Stockel, and C.M. Wayman, eds., *Engineering Applications of Shape Memory Alloys*, Butterworth-Heinemann Applications, London, 1990, p 394
3. P. Ochin, V. Kolomytsev, A. Pasko, P. Vermaut, F. Prima, and R. Portier, Phase Transformations in Rapidly Solidified (Ti-Zr)50(Ni-Cu-Sn)50 Alloys, *Mater. Sci. Eng. A*, 2006, **438–440**, p 630–633
4. S.H. Whang, Ductile, Single Phase-Continuous Super-Conducting Oxide Conductors, U.S. Patent 4,968,663
5. Y.-w. Kim, Y.-m. Yun, and T.-h. Nam, The Effect of the Melt Spinning Processing Parameters on the Solidification Structures in Ti–30 at.% Ni–20 at.% Cu Shape Memory Alloys, *Mater. Sci. Eng. A*, 2006, **438–440**, p 545–548
6. M.J. Kramer, H. Mecco, K.W. Dennis, E. Vargonova, R.W. McCallum, and R.E. Napolitano, Rapid Solidification and Metallic Glass Formation—Experimental and Theoretical Limits, *J. Non-Cryst. Solids*, 2007, **353**, p 3633–3639
7. A. Undisz, S. Flauder, and M. Rettenmayr, Metallographische Präparation und Gefüge von Ni-Ti Legierungen mit Formgedächtnis/Pseudoelastizität, *Prakt. Met. Sonderband*, 2008, **40**, p 331–335 (in German)
8. J. Dutkiewicz, T. Czeppe, and J. Morgiel, Effect of Titanium on Structure and Martensic Transformation in Rapidly Solidified Cu–Al–Ni–Mn–Ti Alloys, *Mater. Sci. Eng. A*, 1999, **273–275**, p 703–707
9. G.A. Lara-Rodriguez, G. Gonzalez, H. Flores-Zúñiga, and J. Cortés-Pérez, The Effect of Rapid Solidification and Grain Size on the Transformation Temperatures of Cu–Al–Be Melt Spun Alloys, *Mater. Charact.*, 2006, **57**, p 154–159